

Computational Modeling of Lauric Acid at the Organic–Water Interface

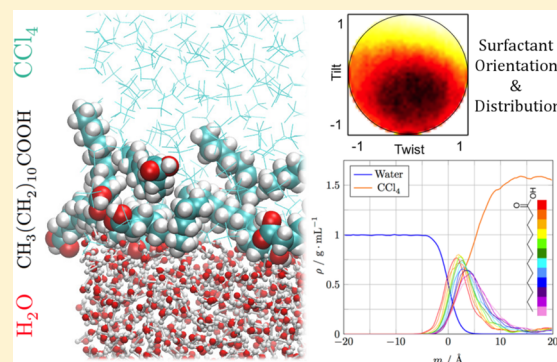
Lars K. Holte,[†] Bryan A. Kuran,[†] Geraldine L. Richmond,*[‡] and Kevin E. Johnson*,[†]

[†]Department of Chemistry, Pacific University, Forest Grove, Oregon 97116, United States

[‡]Department of Chemistry, University of Oregon, Eugene, Oregon 97403, United States

Supporting Information

ABSTRACT: Where water meets an immiscible liquid, the orientation and hydrogen bonding patterns of the molecules nearest the interface differ significantly from those in the bulk. These differences drive important interface-specific phenomena, including interfacial tension and the adsorption of other molecular species. Additionally, surfactants and other amphiphilic molecules present at the interface interact with both the aqueous and hydrophobic layers in a complex fashion that can dramatically change the characteristics of the interface as a whole. In this study, classical molecular dynamics computer simulations have been employed to investigate the accommodation of lauric acid at the water–hexane and water–carbon tetrachloride interfaces. Our results show that the behavior of surfactant molecules in the interfacial region is strongly influenced by the protonation of their headgroups. Deprotonated lauric acid molecules cause a larger increase in interfacial width than their protonated counterparts. The carboxylate headgroups of laurate anions in the interfacial region consistently point toward the water layer, while the orientation of the protonated lauric acid headgroups changes with depth into the water layer.



INTRODUCTION

Water is ubiquitous in our natural environment and is an essential component of all known biological and ecological systems. Ancient philosophers, perceiving its fundamental importance to all of life and nature, assigned it a place among the four “elements”. Today, thousands of years after this speculation, our knowledge of water as a compound has been considerably advanced. Yet many details of its molecular-level structure and dynamics remain a topic of intense interest and debate among scientists.¹ The nature of the interface between water and a hydrophobic substance has been the topic of much research.^{2–8} The water–vapor interface has also been thoroughly investigated theoretically,⁹ computationally,^{10–14} and experimentally.^{10,15–17} The hydrogen bonding patterns^{2,3,14,18} and molecular orientation^{3,8,18} of water molecules in both these interfacial regions differ significantly from those in the bulk. The unique properties of interfacial water can be further modified by surfactants and other amphiphilic species at the interface. Carboxylate surfactants, in particular, play an important role in many industrial and biological processes.¹⁹

In this study we focus on how lauric acid (dodecanoic acid), a 12-carbon, saturated, straight-chain carboxylate surfactant, is accommodated at the interface of water with an immiscible organic component, either *n*-hexane or carbon tetrachloride. We examine the orientation and distribution of the surfactant headgroups as a function of surfactant saturation and protonation. We also look at the effect of increasing surfactant saturation on the width of the interface between the organic

and aqueous layers. Classical molecular dynamics simulations were utilized to obtain a detailed, molecular-level perspective of this chemical system.

COMPUTATIONAL METHOD

A total of 28 classical molecular dynamics computer simulations containing lauric acid surfactants were performed using the Amber 12 software package.²⁰ Each simulation consists of a layer of water in contact with a layer of *n*-hexane or carbon tetrachloride. Surfactant molecules are initially positioned in the organic layer with their carboxylic groups near the organic–water interface. Because atomic polarizability is known to be a significant factor when modeling water,^{21,22} the POL3 polarizable water model²³ was used throughout. Polarizable sodium ion parameters developed by Dang were employed.²⁴ Bonding and van der Waals parameters from the Amber General Force Field for organic compounds²⁵ (Version 1.4) were used with atomic polarizabilities developed by Applequist et al.²⁶ to model hexane and lauric acid. The bonding and van der Waals parameters developed by Schweighofer et al. were used for carbon tetrachloride,²⁷ while the atomic polarizabilities were taken from a previous work by Chang et al.²⁸ To validate this combination of parameters, we performed a simulation of the neat CCl₄–vacuum interface and found the calculated surface

Received: December 7, 2013

Revised: April 15, 2014

Published: April 18, 2014



tension (27.1 ± 0.6 dyn/cm) to be in fairly good agreement with the published value of 26.43 dyn/cm at 25 °C²⁹ (S1, Supporting Information). As previous researchers have done,³⁰ we derive the atomic partial charges for the surfactants from *ab initio* electronic structure calculations. These were performed with the Gaussian 09 software package³¹ (S2, Supporting Information).

Initial Configuration. The initial configuration of each simulation consists of a 40 Å cube of water adjacent to a 40 Å cube of hexane or carbon tetrachloride (Figure 1). The

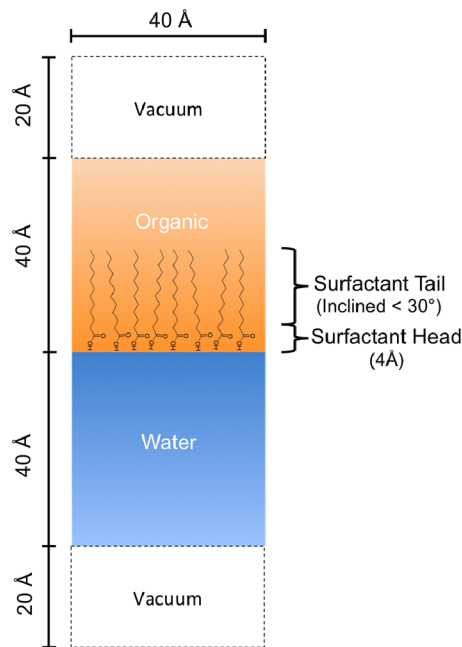


Figure 1. Representative initial configuration.

simulation box is periodic in all directions, effectively extending the cubic sections of water and the organic liquid into infinite contacting slabs. The noncontacting surfaces of the aqueous and organic layers are separated by 40 Å of vacuum. Surfactant molecules are positioned in the organic layer with the carbonyl carbon of each surfactant constrained to reside within 4 Å of the plane of contact between the two liquids. The vector between the tail and head carbons of each surfactant is inclined no more than 30° from an axis perpendicular to the interfacial plane. Previously, we performed simulations in which lauric acid molecules were distributed uniformly in a 40 Å layer of water between two 30 Å CCl_4 layers. The surfactants in these simulations made their way to the water–organic interfaces in less than 1 ns. In the current work, we have positioned the surfactant headgroups near the organic–water interface in the initial configuration in order to reduce the amount of time required for equilibration. Each simulation employed either the protonated or deprotonated form of the surfactant, but not a mixture of the two. This approach allows us to better determine the effect of each species on the interface but neglects effects which may occur due to interaction of the species, such as the acid–anion complex that forms between protonated and deprotonated molecules at the interface in the pH range where both species exist in appreciable quantity.¹⁹ Because of the difficulty of accurately modeling hydronium ions using classical molecular dynamics techniques, aqueous sodium ions serve as the counterion for the deprotonated laurate anions. A

single water molecule was removed from the initial configuration for each sodium ion inserted into the aqueous phase. The molecular coordinates for the initial configuration of each simulation were generated using Packmol software.³²

Simulations were performed with eight different initial surfactant saturations (Table 1). It is important to note that

Table 1. Initial Surfactant Saturations

no. of surfactants	surface excess (10^{14} molecules/cm 2)	% of experimental saturation point
0	0.000	0
1	0.0625	4
6	0.375	25
12	0.750	50
18	1.13	75
24	1.50	100
30	1.88	125
36	2.25	150

the surfactants were not constrained to reside at the interface during coordinate evolution, and thus the saturation could change over the duration of the simulation. In particular, the neutral surfactant molecules were observed to become solvated in the organic phase, effectively decreasing the interfacial saturation (see, for example, Figure 5a). Surface tension measurements have shown the limiting surface coverage for sodium laurate at room temperature at the water– CCl_4 interface to be 67 Å 2 /molecule (1.5×10^{14} molecules/cm 2).¹⁹ The percentages in Table 1 are based off this value. Because the experiments were conducted at a pH of 10 and the p K_a of lauric acid is near 7.48,³³ more than 99% of the bulk surfactant molecules in the experiment are expected to be deprotonated. The saturation point and calculated percentages are therefore most relevant for the simulations of sodium laurate.

Simulation Details. Amber was used to minimize the potential energy of the simulation initial configurations. 800 minimization cycles were performed using the steepest descent method for the first 50 and the conjugate gradient method for the rest. 50 ps of equilibration was carried out with a 1 fs time step, during which time the temperature was elevated to 298 K via Langevin dynamics. The SHAKE algorithm³⁴ was used to constrain bonds involving hydrogen, and the particle mesh Ewald (PME) method³⁵ was used to evaluate electrostatic interactions. Cheng et al. have determined that a VDW cutoff distance of at least 14 Å is required for the calculated surface tension of an interfacial system to stabilize.³⁶ Although we did not perform surface tension calculations for the surfactant-containing simulations in this work, we expect that stabilization of the calculated surface tension may reflect the stabilization of other important interfacial characteristics. For this reason, we have employed a Lennard-Jones cutoff of 14 Å in all our simulations.

After equilibration, 14 ns of evolution was carried out with the same time step. A Langevin dynamics collision frequency of 5 ps $^{-1}$ was employed to maintain the temperature at 298 K. In order to prevent gradual heating of the simulation, we found it necessary to apply a weak temperature control to the molecular dipoles using a Car–Parrinello scheme. The dipoles were assigned a fictitious mass (0.33 kcal ps 2 /D 2) and weakly coupled to a low temperature external bath using the Berendsen weak coupling scheme³⁷ with a large time constant (9.99 ps).³⁸ This issue is described in the Amber 12 manual.²⁰

The analysis and results presented here are based solely on the last 4 ns of the evolution; the initial 10 ns of coordinate evolution was allowed for the interfacial system to reach a steady state.

We compared the positions of the peak sodium ion density and carbonyl carbon density between the first and second halves of our analysis window (10–12 and 12–14 ns). We found that the sodium ion peak shifted no more than 0.9 Å for all simulations with initial saturations less than 1.5×10^{14} molecules/cm². The position of the peak carbonyl carbon density was difficult to estimate for simulations under 7.5×10^{13} molecules/cm², due to the smaller number of surfactants and smaller sampling window. For simulations from 7.5×10^{13} to 1.5×10^{14} molecules/cm², we noted that the carbonyl carbon peak shifted no more than 1.0 Å. This leads us to conclude that the systems with initial saturations less than 1.5×10^{14} molecules/cm² (the experimental saturation point for sodium laurate) are reasonably close to equilibrium. However, we obtained irregular orientation profiles for simulations of sodium laurate at saturations greater than this value, suggesting that these systems may require more time to reach a steady state and that our sampling window needs to be extended beyond 4 ns to adequately sample all states of the equilibrium.

Aqueous Surface Location. The organic–water interface within each simulation is a dynamic boundary that may be neither flat nor stationary. Molecules from one phase are spatially displaced by molecules of the other, causing the surface of contact between the two interfacial liquids to deviate from a plane. A region of overlap in the density of the interfacial liquids occurs as a result, in which the density of water changes from its bulk value to zero. Previous studies have computed the density of water along the axis of the simulation which passes through the bulk of both liquids then fit the resulting curve to a hyperbolic tangent function.^{8,14} The best-fit parameters for this function provide a quantitative measure of the breadth of the water density curve and hence suggest the magnitude of the overlap in the densities of the two phases, which we term the “interfacial width”. Large-scale features of interfacial morphology, such as capillary waves, serve to increase interfacial width, as do smaller spatial displacements between the molecules at the fringe of each phase. It is impossible to distinguish between these two contributing factors based solely on the density profile. Additionally, because the water density is averaged over the duration of the simulation, the region of overlap will be broadened not only by irregular surface features but also by any systematic drift of the simulation along the axis perpendicular to the interface. In an effort to reduce uncontrolled drift, we set the center of mass of each of our simulations to the origin every picosecond. To further mitigate the effects of surface drift on our analysis, we chose to take the approach outlined by Shamay et al. in 2011: define a mobile reference point in the interfacial region to serve as an estimate of aqueous surface location at each time step.³⁹ We calculate this reference position by averaging the z-coordinate of the uppermost 124 water molecules in each frame of the simulation. (The number 124 was based on an estimate of the number of molecules in a monolayer in a simulation of our size. It is not critical that this number accurately reflect the amount of water in a single layer nearest the organic phase, but it is critical that it serve as a repeatable estimate of aqueous surface location.) This reference position is taken as the zero point of a movable axis termed the *interfacial axis* or the *axis of interfacial position* (*m*). The interfacial axis is parallel to the z-axis but moves according to

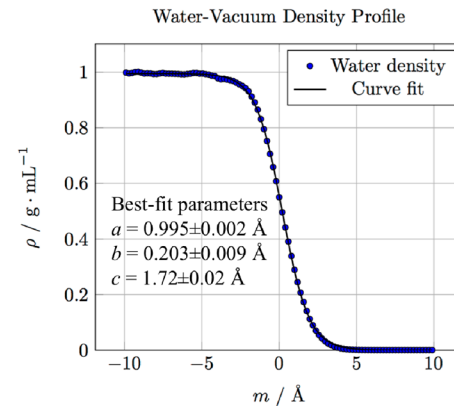


Figure 2. The calculated density of water at the water–vacuum interface and the best-fit curve based on eq 1.

the location of the water layer at each time step. It is therefore better able to represent displacement from the surface of contact between the two liquids.

RESULTS AND DISCUSSION

Interfacial Width. We performed simulations of the neat water–vacuum interface and the neat water–organic interfaces in addition to those containing surfactants. The setup parameters for these simulations were identical to those described above except for the omission of surfactants from the initial configuration and the omission of the organic layer from the simulation of the water–vacuum interface. Coordinate evolutions for these simulations were carried out to 4 ns, and statistics were collected over the entire evolution. Our intent in performing these simulations was to provide a comparison for the surfactant-containing simulations, particularly in terms of interfacial width. We quantify the width of the interfacial region using a best-fit curve for the water density profile based on the hyperbolic tangent function:

$$\rho(m) = \frac{a}{2} \left(1 - \tanh\left(\frac{m - b}{c}\right) \right) \quad (1)$$

Here *m*, interfacial position, is the independent variable, while *a*, *b*, and *c* are best-fit parameters. *a* is the maximum height of the curve fit, corresponding to the bulk density of water; *b* is the center (inflection) point of the water density profile in the interfacial region; and *c* is a measure of the width of the interface: 80% of the density change occurs within $2 \tanh^{-1}(0.8)c \approx 2.20c$ of the inflection point, making 2.20c the 90–10 width. For the water–vacuum profile, *b* is also the location of the Gibbs dividing surface.⁴⁰ The best-fit parameters were calculated from the water density data in each simulation using Numerical Python⁴¹ (S3, Supporting Information).

The width of the water–CCl₄ interface (*c* = 1.73 ± 0.03 Å) is similar to that of the water–vacuum interface (*c* = 1.72 ± 0.02 Å), while the water–hexane interface is significantly wider (*c* = 1.92 ± 0.02 Å, a 90–10 width of 4.22 ± 0.04 Å). Mitrinovic et al. have determined the interfacial width (σ in the classical capillary wave model) of the water–hexane interface to be 3.3 ± 0.25 Å using X-ray reflectivity experiments.⁴² This corresponds to a 90–10 width of 8.5 ± 0.7 Å, which is significantly larger than our calculated value. We attribute this difference to the fact that our simulation box is not large enough in the *X* and *Y* dimensions to account for the thermally induced capillary waves that would be present in a real system.

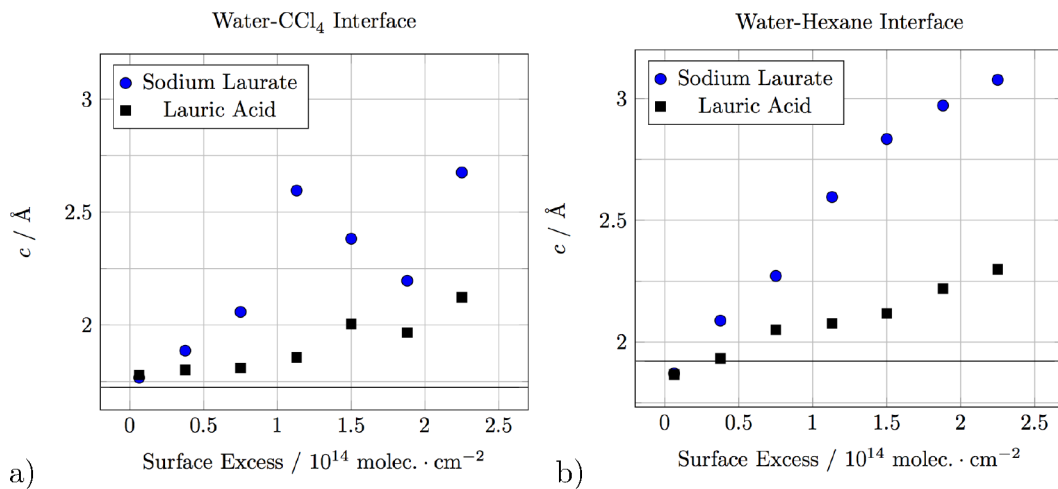


Figure 3. Best-fit c (interfacial width) parameters as a function of initial surfactant surface excess for the water-CCl₄ (a) and water-hexane (b) interfaces. The black horizontal line in each plot represents the c parameter for the neat water-organic interface.

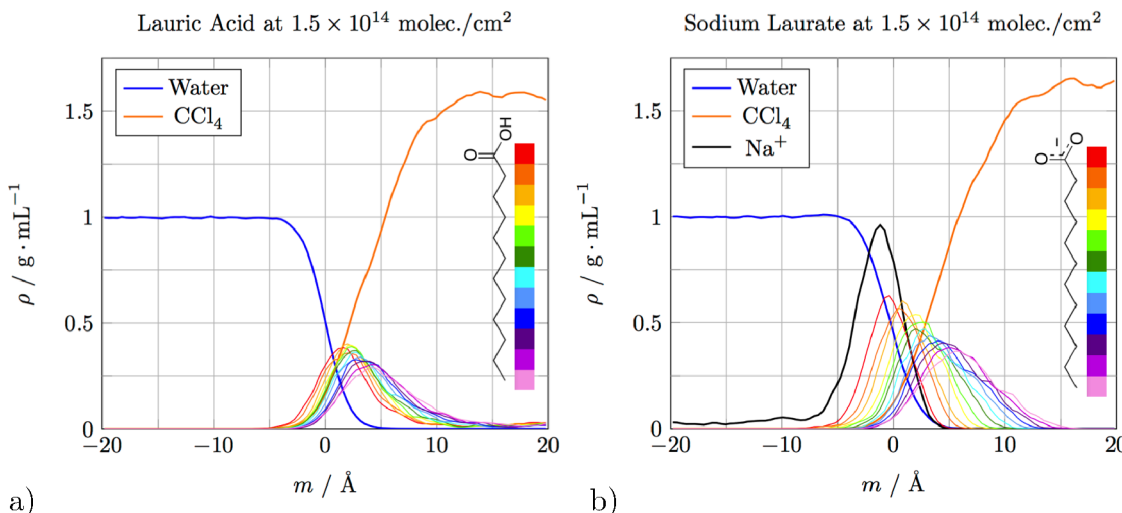


Figure 4. Density distributions are shown for each carbon in lauric acid (a) and laurate (b) from the carbonyl carbon (red) to the tail carbon (pink) in simulations of both species at 1.5×10^{14} molecules/cm² at the water-CCl₄ interface. Surfactant carbon atom and sodium ion densities are scaled by a factor of 10 for visibility.

Our results are similar to those obtained by other researchers using classical molecular dynamics methods.⁴³

Figure 3 plots the value of c for surfactant-containing simulations of the water-CCl₄ and water-hexane interfaces. A significant increase in interfacial width is observed with increasing concentration of the anionic form of the surfactant at both the water-hexane and water-CCl₄ interfaces. There is a much smaller increase in interfacial width associated with increasing concentration of protonated lauric acid molecules. We hypothesize that the deprotonated, anionic headgroups at both water-hexane and water-CCl₄ interfaces repel each other electrostatically, assuming a nonplanar configuration in order to maximize the distance between neighboring charged headgroups, yet each carboxylate group remains attracted to the water layer due to water's ability to stabilize its negative charge. The combination of long-range repulsion among the headgroups with short-range attraction to the water phase may cause the interface to deform vertically, resulting in the observed increase in interfacial width.

Interfacial width increases uniformly with surfactant saturation at the water-hexane interface but shows significant

variation at the water-CCl₄ interface, particularly for the dissociated, anionic form of the surfactant. The interfacial width of this system is observed to increase just below the saturation point of 1.5×10^{14} molecules/cm² and then to decrease above the saturation point. Both changes are sufficiently large to reverse the trend in width for saturations near 1.5×10^{14} molecules/cm². The fit of the water density curve to the hyperbolic tangent function in each case is quite precise ($c = 2.60 \pm 0.06$ Å for 1.13×10^{14} molecules/cm² and 2.20 ± 0.05 Å for 1.88×10^{14} molecules/cm²). However, in order to determine the uncertainty of c , replicate simulations at each saturation would be required. These results suggest that a preliminary evolution of more than 10 ns may be required for laurate-containing simulations to reach a steady state.

Surfactant Distribution. The penetration of the surfactant headgroup into the aqueous layer was observed to vary according to surfactant protonation and interfacial saturation. To quantify the depth of surfactant headgroup penetration and tail conformation, we plotted the density of each carbon in the surfactant molecules separately (Figure 4).

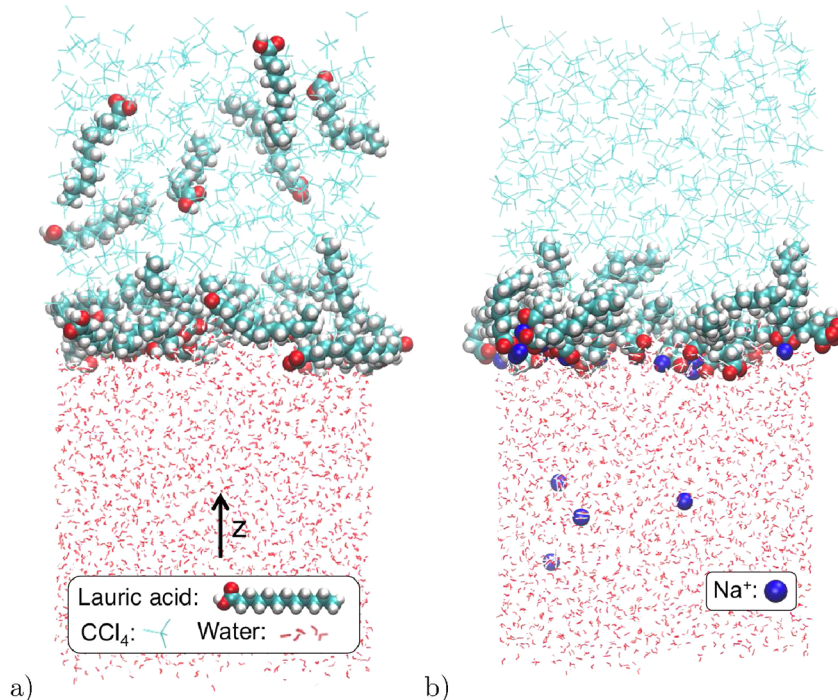


Figure 5. Simulation visualizations⁴⁴ showing the distributions of protonated (a) and deprotonated (b) surfactants at 1.5×10^{14} molecules/cm² at the water–CCl₄ interface. The broad distribution of lauric acid molecules into the organic layer is evident, as is laurate’s tendency to remain near the interface. The tails of the deprotonated surfactants are observed to align more nearly normal to the interfacial plane than their protonated counterparts.

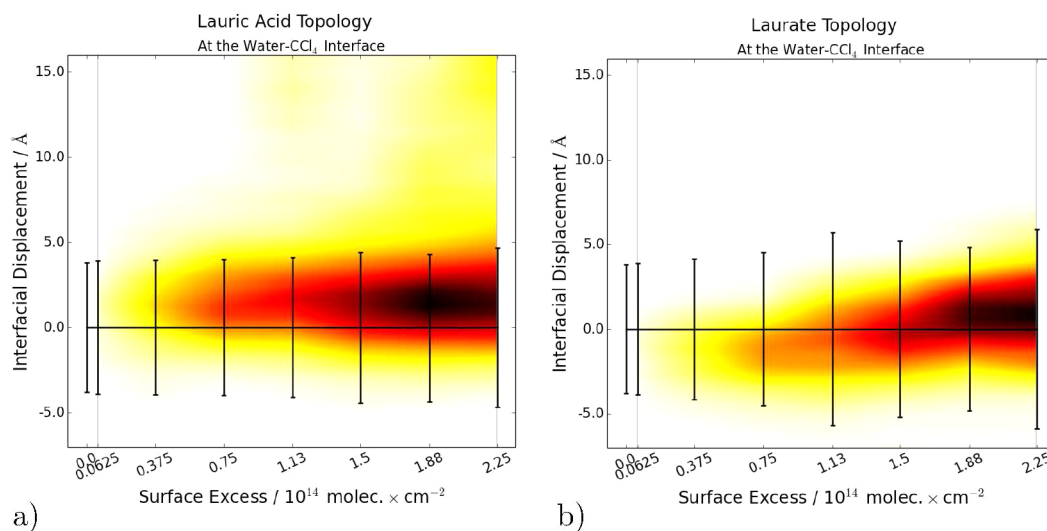


Figure 6. Carbonyl carbon distribution at the water–CCl₄ interface. The vertical axis (interfacial displacement) differs from interfacial position (m) for each simulation as described in the text. The horizontal black line marks the inflection point of the water density function for each saturation, while the vertical black lines show the region $2.20c$ on either side. The vertical black lines mark the 90–10 width of the water density curve for each saturation.

A comparison of the carbon density distributions along the interfacial axis for lauric acid and sodium laurate (Figure 4) shows that the deprotonated surfactant headgroups penetrate farther into the water layer than the protonated ones. Additionally, there is a residual density of the protonated surfactant molecules which continues more than 20 Å into the CCl₄ layer, while the laurate carbon densities remain within ~15 Å of the interface. For both forms of the surfactant, the peak carbon densities assume a nearly consecutive ordering in terms of interfacial position, with carbons closer to the

headgroup remaining nearer the water. The peak position of the carbon density curves from head to tail changes much less for lauric acid (around 2.8 Å in Figure 4) than for the laurate (around 5.9 Å). This suggests that the laurate tails tend to orient more nearly normal to the interfacial plane than those of lauric acid. A slight difference in preferred orientation is noticeable upon comparison of Figure 5a,b.

To better visualize the location of the surfactant headgroups as a function of their protonation and saturation, we created topological plots of the carbonyl carbon density distributions

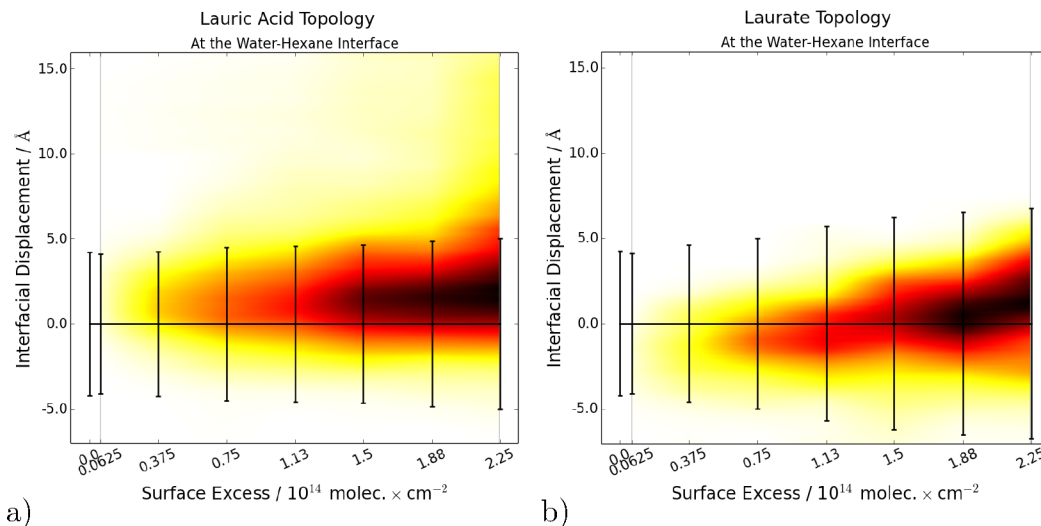


Figure 7. Carbonyl carbon distribution at the water–hexane interface. These plots were generated as described for Figure 6. The difference in carbonyl carbon distribution between the water–hexane and water– CCl_4 interfaces appears to be less significant than the difference caused by protonation of the surfactants.

for varying initial surface saturations (Figures 6 and 7). The darkest region of each plot represents the highest carbonyl carbon density, while the lightest region represents the lowest density. White regions represent a density of zero, indicating that no surfactant heads were observed. The vertical axis on these graphs, “interfacial displacement”, is parallel to the interfacial axis (m) described previously but has been translated so that zero corresponds to the water density curve inflection point (b in eq 1) for each saturation. This was necessary because the broadening of the water density curve with increasing saturation caused an increase in the displacement between $m = 0$ and the density function inflection point.

Figure 6 shows the distribution of carbonyl carbons, and, by extension, surfactant headgroups, at the water– CCl_4 interface. Many of the protonated surfactants become solvated in the organic layer, as evidenced by the large, lightly colored region at high values of interfacial displacement in Figure 6a. Laurate’s headgroup distribution, by contrast, is much narrower. The increased area of the dark region beneath the horizontal black line (water density inflection point) in Figure 6b shows that the anionic form of the surfactant penetrates farther into the aqueous layer than the acidic form, an effect that was also noticeable in the carbon density profiles of the interfacial region (Figure 4). Laurate’s electrostatic attraction to the sodium ions in the water layer may be a factor in causing the deeper distribution of anionic headgroups. Water is better able to stabilize the negative charge on the carboxylate group, which may make interfacial positions within the water layer enthalpically more favorable. Penetration of the aliphatic carbon tail into the water layer disrupts water’s strong hydrogen bonding network, however, which is enthalpically unfavorable. We hypothesize that the combination of these opposing factors draws the anionic headgroups into a fairly narrow region where they can interact with the water layer without drawing the surfactant tail out of the organic.

Overall, the trends for the water–hexane interface (Figure 7) are similar to those for the water– CCl_4 interface. For lauric acid at both the water–hexane and water– CCl_4 interfaces, the interfacial displacement of the peak carbonyl carbon density (the darkest region of the plot) does not change much with an

increase in the number of simulated surfactants. However, for sodium laurate, the darkest region of the graph moves to higher interfacial positions with increasing saturation. The repulsive interactions of the charged laurate headgroups are conducted more effectively through polarizable water, which may account for the limited number of headgroups that appear in regions where there is significant water density, and the resulting upward shift of peak carbonyl density in terms of interfacial position.

Surfactant Headgroup Orientation. Understanding the orientation of water and other species at the organic–water interface is crucial to understanding the interface as a whole. Yet the orientation of even small molecules and functional groups can be difficult to quantify and represent on paper. To simplify this problem, many researchers^{10,39} ignore the rotation of each molecule about the axis perpendicular to the interfacial plane (the z -axis). This is an acceptable simplification to make when collecting aggregate statistics about molecular orientation because the simulation is assumed to be isotropic about that axis.

We have developed a method of mapping all possible orientations of a nonlinear three-atom group relative to a planar interface onto the interior of a circle (Figure 8). The circle is then colored⁴⁵ to represent the number of occurrences of each configuration in a given simulation, with darker colors indicating a high probability and lighter colors a low one. This technique is advantageous in that it intuitively maps several key orientations of the group to prominent places on the circle (i.e., its left, right, top, bottom, and center). The carbonyl carbon, carbonyl oxygen, and acid oxygen are taken as the three reference atoms for each surfactant in our simulations. The top and bottom of the circular histogram represent configurations where the headgroup bisector (\vec{B}) points directly into the organic or directly into the water, respectively. Along the horizontal diameter of the circle, the bisector is parallel to the interfacial plane. The left and right sides of the histogram, in this case, are differentiated by whether the carbonyl oxygen or acid oxygen points toward the water layer. At the very center of the circle, all three reference atoms are in a plane parallel to the interfacial one, meaning that the surfactant headgroup lies

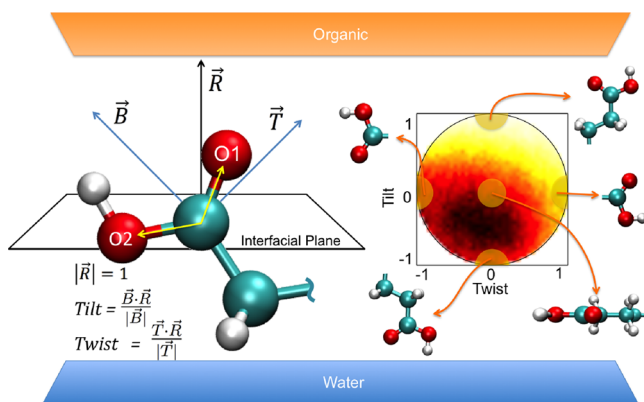


Figure 8. A visual demonstration of the vectors used to calculate surfactant headgroup orientation and the circular histogram on which each headgroup's orientation is plotted. Darker regions within the histogram represent a high probability of occurrence of those orientations, while lighter regions represent a low probability. White regions indicate that no surfactants were found to have a particular orientation. All possible orientations of a nonlinear three-atom group map into the circular region of the histogram outlined in black.

"flat" on the interface. See the Supporting Information (S4) for a detailed description of how the histogram is generated.

We divide the interfacial region of each simulation into 16 evenly spaced slices along the interfacial axis (m) and analyze the orientation of the headgroups in each one individually. A separate orientation histogram is calculated for each slice based on all the surfactant headgroups whose carbonyl carbons fall inside that slice, and the resulting plots are arranged in a grid. Figure 9 shows one such grid for a simulation of sodium laurate

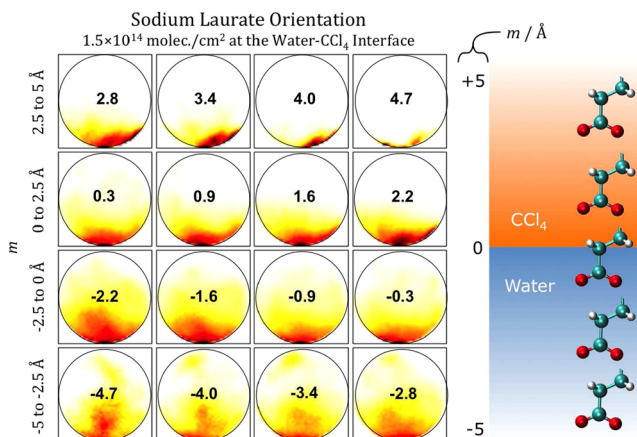


Figure 9. A visual representation of the orientation of sodium laurate at 1.5×10^{14} molecules/cm² at the water-CCl₄ interface. On the left are the orientation histograms for surfactants in each slice of the interface. Histograms are arranged first left to right and then bottom to top with increasing interfacial position. The number at the center of each histogram denotes the midpoint of the range along the interfacial axis (m/Å) for that slice. On the right is a graphical interpretation of the data.

at 1.5×10^{14} molecules/cm² at the water-CCl₄ interface. Because the second and third reference atoms (the carboxylate oxygens) are chemically equivalent, the histograms have a vertical line of symmetry: values on the right side of the graph mirror values on the left. The most highly populated region is at the bottom of each circular plot, indicating that the

headgroup bisector tends to point into the aqueous layer, regardless of depth. This is consistent with our previous observation of the ordering of laurate carbon densities at the interface. It also suggests that the anionic headgroup's orientation in the interfacial region is governed by its electrostatic attraction to the sodium ions in the water layer. Recent sum frequency generation experiments also indicate that the bisectors of laurate headgroups tend to align perpendicular to the interfacial plane.¹⁹ This trend is consistent for saturations under 1.5×10^{14} molecules/cm² at both the water-Cl₄ and water-hexane interfaces. Above this saturation, the trends are irregular, and the asymmetry of histograms generated indicates that a larger sampling window may be required.

For protonated lauric acid molecules, the results are quite different (Figure 10). More than about 4 Å into the organic

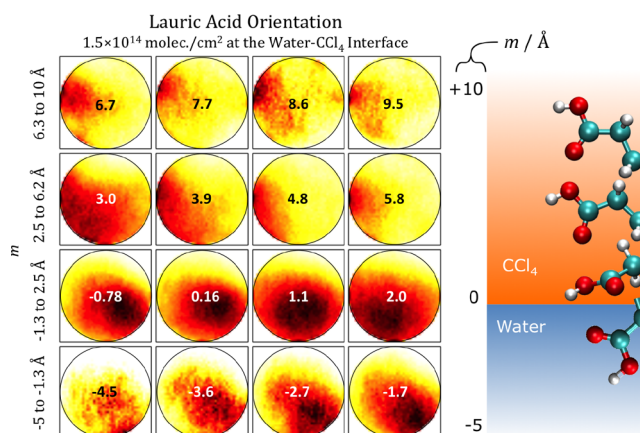


Figure 10. A visual representation of the orientation of lauric acid at 1.5×10^{14} molecules/cm² at the water-CCl₄ interface. The histograms are arranged as described in Figure 9, and a graphical interpretation of the results is given on the right.

layer, the highest density is at the left of each histogram, indicating that many headgroups orient with their bisectors parallel to the interfacial plane and with their carbonyl oxygen tilted down. Nearer the interface (from about $m = 2-4$ Å) the density shifts to the bottom left of the histogram. This indicates that the carbonyl oxygen continues to point more or less toward the water layer while the headgroup tilts downward. Color density in the orientation histogram centered around $m = 1.1$ Å tends toward the bottom of the plot, but the very bottom is sparsely populated. This indicates that while many surfactants tilt toward the water layer at this level, few point directly into the water layer. The color density of this graph has also moved to the horizontal center, indicating that neither the carbonyl nor the acid oxygen preferentially points toward the water layer. Below this point there is a growing downward and rightward trend in the histograms. The downward trend is likely caused by the hydrophobic surfactant tail, which orients the base of the headgroup (the carbonyl carbon) toward the organic. The rightward trend indicates that there is a preference for the carbonyl oxygen to remain tilted toward the organic. From this we can note that the carbonyl oxygen tends to point toward the meeting of the immiscible liquids, whether it is in the aqueous or the organic layer. Additional studies of the electric field and hydrogen bonding at the interface may be required to elucidate the origin of this effect. These general trends are consistent for lauric acid between the water-CCl₄ and water-hexane for saturations at or above 7.5×10^{13} molecules/cm². Below this

value, there is not enough data in our 4 ns sampling window to draw precise conclusions about lauric acid headgroup orientation.

Comparison with VSFS Experiments. It is interesting to compare the results of these calculations with recent sum frequency spectroscopic (VSFS) studies of lauric acid at the water–CCl₄ interface.¹⁹ In these studies, both the carboxylate/carboxylic acid headgroup and the CH modes of the alkyl chains were monitored upon variation of the pH and surfactant concentration. With VSFS, surfactants can only be observed at this interface if they adsorb with the molecular moieties probed having a net orientation relative to the interface.⁴⁶ When the surfactant is deprotonated at high pH, the carboxylate mode shows a strong net orientation perpendicular to the plane of the interface. The alkyl CH modes are also observed yet display significant gauche defects in the backbone. At low pH where the surfactant is largely protonated, the VSF signal from the carboxylic acid group is barely observable which the authors attribute to a low concentration of oriented surfactants at the interface. The alkyl chains are not observable at this low pH. The results of these simulations indicate, however, that there may be a considerable number of lauric acid molecules present at the interface. Unlike the ordered interfacial structure of the deprotonated surfactants, the protonated surfactants have a broad range of orientations. This type of orientation at the interface would cause the surfactant modes to be barely sum-frequency active, as is observed. The surface tension measurements conducted in conjunction with the VSF experiments indicate that at pH above ~5 the presence of the surfactant causes a significant drop in the surface tension. Below that pH, however, the drop in surface tension is negligible. Our calculations indicate that the lack of a drop in surface tension at low pH is not a result of a significant loss in surfactant surface concentration, but more a result of the limited energetically favorable cohesive interactions between water and the hydrophilic carboxylic headgroups as well as between the adjacent adsorbed surfactant molecules.⁴⁷

CONCLUSION

The width of the water–hexane and water–CCl₄ interfaces increases significantly with increasing saturation of sodium laurate, but only slightly with increasing saturation of lauric acid. Electrostatic repulsion among the charged laurate headgroups may account for this difference. Protonation is also an important factor in determining the depth of penetration of carboxylate surfactant headgroups into the water layer, with deprotonated surfactants penetrating farther into the water layer than lauric acid, and not becoming solvated in the organic phase. The orientation of negatively charged carboxylate headgroups remains uniform at saturations less than 1.5×10^{14} molecules/cm² near the water–hexane and water–CCl₄ interfaces, suggesting that the orientation of these functional groups is governed by electrostatic attraction to sodium ions in the water. The orientation of protonated lauric acid headgroups, however, does change with depth. In the layer of organic nearest the water, the carbonyl oxygen tends to point toward the aqueous layer. As surfactant headgroups penetrate farther into the water layer, they tilt so that the base of the headgroup (the carbonyl carbon) remains nearer the organic layer, which we attribute to the hydrophobic tail's affinity for the organic layer. Once within the water layer, the surfactants reorient again so that the carbonyl oxygen points toward the organic. The fact that the orientation of lauric acid changes

substantially in the interfacial region while the orientation of sodium laurate remains relatively constant is consistent with experimental VSFS results.

ASSOCIATED CONTENT

S Supporting Information

A detailed explanation of the surface tension calculation for the CCl₄–vacuum interface, optimization of the surfactant structure, water density curve fitting, and generation of the orientation histograms. This material is available free of charge via the Internet at <http://pubs.acs.org>.

AUTHOR INFORMATION

Corresponding Authors

*E-mail richmond@uoregon.edu (G.L.R.).

*E-mail johnsonk@pacificu.edu (K.E.J.).

Notes

The authors declare no competing financial interest.

ACKNOWLEDGMENTS

We gratefully acknowledge the support of the M. J. Murdock Charitable Trust and Pacific University. The computational resources of the University of Oregon Applied Computation Instrument for Scientific Synthesis (ACISS, NSF Grant OCI-0960354) were also appreciated. This material is based upon work supported by the National Science Foundation under CHE-0652531.

REFERENCES

- (1) Ball, P. Water as an Active Constituent in Cell Biology. *Chem. Rev.* **2008**, *108*, 74–108.
- (2) Benjamin, I. Theoretical Study of the Water/1,2-Dichloroethane Interface: Structure, Dynamics, and Conformational Equilibria at the Liquid-Liquid Interface. *J. Chem. Phys.* **1992**, *97*, 1432–45.
- (3) Chang, T.-M.; Dang, L. X. Molecular Dynamics Simulations of CCl₄–H₂O Liquid-Liquid Interface with Polarizable Potential Models. *J. Chem. Phys.* **1996**, *104*, 6772–83.
- (4) Scatena, L. F.; Richmond, G. L. Orientation, Hydrogen Bonding, and Penetration of Water at the Organic/Water Interface. *J. Phys. Chem. B* **2001**, *105*, 11240–50.
- (5) Chowdhary, J.; Ladanyi, B. M. Water-Hydrocarbon Interfaces: Effect of Hydrocarbon Branching on Interfacial Structure. *J. Phys. Chem. B* **2006**, *110*, 15442–53.
- (6) Hore, D. K.; Walker, D. S.; MacKinnon, L.; Richmond, G. L. Molecular Structure of the Chloroform-Water and Dichloromethane-Water Interfaces. *J. Phys. Chem. C* **2007**, *111*, 8832–42.
- (7) Hore, D. K.; Walker, D. S.; Richmond, G. L. Water at Hydrophobic Surfaces: When Weaker is Better. *J. Am. Chem. Soc.* **2008**, *130*, 1800–01.
- (8) Shamay, E. S.; Richmond, G. L. Ionic Disruption of the Liquid-Liquid Interface. *J. Phys. Chem. C* **2010**, *114*, 12590–97.
- (9) Morita, A.; Hynes, J. T. A Theoretical Analysis of the Sum Frequency Generation Spectrum of the Water Surface. *Chem. Phys.* **2000**, *258*, 371–90.
- (10) Fan, Y.; Chen, X.; Yang, L.; Cremer, P. S.; Gao, Y. Q. On the Structure of Water at the Aqueous/Air Interface. *J. Phys. Chem. B* **2009**, *113*, 11672–79.
- (11) Wick, C. D. Hydronium Behavior at the Air-Water Interface with a Polarizable Multistate Empirical Valence Bond Model. *J. Phys. Chem. C* **2012**, *116*, 4026–38.
- (12) Dang, L. X.; Chang, T.-M. Molecular Dynamics Study of Water Clusters, Liquid, and Liquid-Vapor Interface of Water with Many-Body Potentials. *J. Chem. Phys.* **1997**, *106*, 8149–59.
- (13) Mundy, C. J.; Kuo, I.-F. W. First-Principles Approaches to the Structure and Reactivity of Atmospherically Relevant Aqueous Interfaces. *Chem. Rev.* **2006**, *106*, 1282–304.

- (14) Kühne, T. D.; Pascal, T. A.; Kaxiras, E.; Jung, Y. New Insights into the Structure of the Vapor/Water Interface from Large-Scale First-Principles Simulations. *J. Phys. Chem. Lett.* **2011**, *2*, 105–13.
- (15) Shen, Y. R.; Ostroverkhov, V. Sum-Frequency Vibrational Spectroscopy on Water Interfaces: Polar Orientation of Water Molecules at Interfaces. *Chem. Rev.* **2006**, *106*, 1140–54.
- (16) Richmond, G. L. Molecular Bonding and Interactions at Aqueous Surfaces as Probed by Vibrational Sum Frequency Spectroscopy. *Chem. Rev.* **2002**, *102*, 2693–724.
- (17) Gan, W.; Wu, D.; Zhang, Z.; ran Feng, R.; Wang, H.-f. Polarization and Experimental Configuration Analyses of Sum Frequency Generation of Vibrational Spectra, Structure, and Orientational Motion of the Air-Water Interface. *J. Chem. Phys.* **2006**, *124*, 114705–20.
- (18) Linse, P. Monte Carlo Simulation of Liquid-Liquid Benzene-Water Interface. *J. Chem. Phys.* **1987**, *86*, 4177–87.
- (19) Beaman, D. K.; Robertson, E. J.; Richmond, G. L. From Head to Tail: Structure, Solvation, and Hydrogen Bonding of Carboxylate Surfactants at the Organic-Water Interface. *J. Phys. Chem. C* **2011**, *115*, 12508–16.
- (20) Case, D. A.; et al. AMBER 12. 2012, University of California, San Francisco.
- (21) Dang, L. X. Importance of Polarization Effects in Modeling the Hydrogen Bond in Water Using Classical Molecular Dynamics Techniques. *J. Phys. Chem. B* **1998**, *102*, 620–24.
- (22) Rivera, J. L.; Starr, F. W.; Paricaud, P.; Cummings, P. T. Polarizable Contributions to the Surface Tension of Liquid Water. *J. Chem. Phys.* **2006**, *125*, 094712.
- (23) Caldwell, J. W.; Kollman, P. A. Structure and Properties of Neat Liquids Using Nonadditive Molecular Dynamics: Water, Methanol, and N-Methylacetamide. *J. Phys. Chem.* **1995**, *99*, 6208–19.
- (24) Dang, L. X. Computational Study of Ion Binding to the Liquid Interface of Water. *J. Phys. Chem. B* **2002**, *106*, 10388–94.
- (25) Wang, J.; Wolf, R. M.; Caldwell, J. W.; Kollman, P. A.; Case, D. A. Development and Testing of a General Amber Force Field. *J. Comput. Chem.* **2004**, *25*, 1157–74.
- (26) Applequist, J.; Carl, J. R.; Fung, K.-K. An Atom Dipole Interaction Model for Molecular Polarizability. Application to Polyatomic Molecules and Determination of Atom Polarizabilities. *J. Am. Chem. Soc.* **1972**, *94*, 2952–60.
- (27) Schweighofer, K. J.; Essmann, U.; Berkowitz, M. Simulation of Sodium Dodecyl Sulfate at the Water-Vapor and Water-Carbon Tetrachloride Interfaces at Low Surface Coverage. *J. Phys. Chem. B* **1997**, *101*, 3793–99.
- (28) Chang, T.-M.; Peterson, K. A.; Dang, L. X. Molecular Dynamics Simulations of Liquid, Interface, and Ionic Solvation of Polarizable Carbon Tetrachloride. *J. Chem. Phys.* **1995**, *103*, 7502–13.
- (29) Lide, D. R., Haynes, W. M., Eds.; CRC Handbook of Chemistry and Physics; CRC Press: Boca Raton, FL, 2009.
- (30) Brown, M. G.; Walker, D. S.; Raymond, E. A.; Richmond, G. L. Vibrational Sum-Frequency Spectroscopy of Alkane/Water Interfaces: Experiment and Theoretical Simulation. *J. Phys. Chem. B* **2003**, *107*, 237–44.
- (31) Frisch, M. J.; et al. Gaussian 09, Revision B.01; Gaussian Inc.: Wallingford, CT, 2009.
- (32) Martínez, L.; Andrade, R.; Birgin, E. G.; Martínez, J. M. PACKMOL: A Package for Building Initial Configurations for Molecular Dynamics Simulations. *J. Comput. Chem.* **2009**, *30*, 2157–64.
- (33) Kanicky, J. R.; Poniatowski, A. F.; Mehta, N. R.; Shah, D. O. Cooperativity among Molecules at Interfaces in Relation to Various Technological Processes: Effect of Chain Length on the pK_a of Fatty Acid Salt Solutions. *Langmuir* **2000**, *16*, 172–77.
- (34) Ryckaert, J.; Ciccotti, G.; Berendsen, H. Numerical Integration of the Cartesian Equations of Motion of a System with Constraints: Molecular Dynamics of *n*-Alkanes. *J. Comput. Phys.* **1977**, *23*, 327–41.
- (35) Darden, T.; York, D.; Pedersen, L. Particle Mesh Ewald: An $N \cdot \log(N)$ Method for Ewald Sums in Large Systems. *J. Chem. Phys.* **1993**, *98*, 10089–92.
- (36) Cheng, T.; Chen, Q.; Li, F.; Sun, H. Classic Force Field for Predicting Surface Tension and Interfacial Properties of Sodium Dodecyl Sulfate. *J. Phys. Chem. B* **2010**, *114*, 13736–44.
- (37) Berendsen, H. J. C.; Postma, J. P. M.; van Gunsteren, W. F.; DiNola, A.; Haak, J. R. Molecular Dynamics with Coupling to an External Bath. *J. Chem. Phys.* **1984**, *81*, 3684–90.
- (38) Toukmaji, A.; Sagui, C.; Board, J.; Darden, T. Efficient Particle-Mesh Ewald Based Approach to Fixed and Induced Dipolar Interactions. *J. Chem. Phys.* **2000**, *113*, 10913–27.
- (39) Shamay, E. S.; Johnson, K. E.; Richmond, G. L. Dancing on Water: The Choreography of Sulfur Dioxide Adsorption to Aqueous Surfaces. *J. Phys. Chem. C* **2011**, *115*, 25304–14.
- (40) Hiemenz, P. C.; Rajagopalan, R. *Principles of Colloid and Surface Chemistry*, 3rd ed.; CRC Press: Boca Raton, FL, 1997.
- (41) Oliphant, T. Python for Scientific Computing. *Comput. Sci. Eng.* **2007**, *9*, 10–20.
- (42) Mitrinovic, D. M.; Zhang, Z.; Williams, S. M.; Huang, Z.; Schlossman, M. L. X-ray Reflectivity Study of the Water-Hexane Interface. *J. Phys. Chem. B* **1999**, *103*, 1779–82.
- (43) Rivera, J. L.; McCabe, C.; Cummings, P. T. Molecular Simulations of Liquid-Liquid Interfacial Properties: Water-*n*-Alkane and Water-Methanol-*n*-Alkane Systems. *Phys. Rev. E* **2003**, *67*, 011603.
- (44) Humphrey, W.; Dalke, A.; Schulten, K. VMD - Visual Molecular Dynamics. *J. Mol. Graphics* **1996**, *14*, 33–38.
- (45) Hunter, J. D. Matplotlib: A 2D Graphics Environment. *Comput. Sci. Eng.* **2007**, *9*, 90–95.
- (46) Richmond, G. L. Structure and Bonding of Molecules at Aqueous Surfaces. *Annu. Rev. Phys. Chem.* **2001**, *52*, 357–89.
- (47) Davies, J. T.; Rideal, E. K. *Interfacial Phenomena*, 2nd ed.; Academic Press: New York, 1963.